Journal of
Marine Science and Engineering

MDPI

Article

Fault Characteristics and Reservoir Potential of Mesozoic Basins in the Southern East China Sea

Yanqiu Yang [1,2], Chuansheng Yang [1,2], Jing Sun [1,2], Jie Liang [1,2], Qingfang Zhao [1,2,*] and Jianqiang Wang [1,2,*]

[1] Qingdao Institute of Marine Geology, China Geological Survey, Qingdao 266071, China; qimgyyq@126.com (Y.Y.); ychuansheng@mail.cgs.gov.cn (C.Y.); sunjing@mail.cgs.gov.cn (J.S.); cgsljie@mail.cgs.gov.cn (J.L.)
[2] Laboratory for Marine Mineral Resources, Qingdao Marine Science and Technology Center, Qingdao 266071, China
* Correspondence: zqingfang@mail.cgs.gov.cn (Q.Z.); wangjianqiang163@163.com (J.W.)

Abstract: The East China Sea Basin (ECSB) is an integral part of the Western Pacific tectonic system. Its development is linked to the Kula–Pacific Plate and the formation and expansion of the Philippine Sea Basin. Recent advancements in exploration technologies and theory have been applied to Mesozoic basins in the East China Sea. Researchers have posited that the southern basin has great oil and gas exploration potential. However, the characteristics and evolution of fault structures and their influence on hydrocarbon accumulation remain unclear. Here, in-depth geometric and kinematic analyses of Mesozoic fault structures in the southern ECSB were conducted using the latest interpretations of 2D seismic data and structural analysis theory. The findings revealed that the fault system was well developed and predominantly exhibited multiphase extensional and extensional-torsional features. Based on their lateral distribution and morphology, faults were categorized into three structural styles and seven combinations. According to their developmental timing, periods of active faulting were attributed to the Yanshan and Himalayan epochs. Multiphase fault activities strongly controlled the formation of traps and thus hydrocarbon accumulation, while earlier NE-trending faults controlled the formation of structural belts and hydrocarbon source areas.

Keywords: East China Sea; basin analysis; fault characteristics; reservoir potential; hydrocarbon accumulation; Mesozoic; Eurasian Plate; South China Craton

check for updates

Citation: Yang, Y.; Yang, C.; Sun, J.; Liang, J.; Zhao, Q.; Wang, J. Fault Characteristics and Reservoir Potential of Mesozoic Basins in the Southern East China Sea. *J. Mar. Sci. Eng.* **2024**, *12*, 1800. https://doi.org/10.3390/jmse12101800

Received: 19 August 2024
Revised: 29 September 2024
Accepted: 8 October 2024
Published: 9 October 2024

Copyright: © 2024 by the authors. Licensee MDPI, Basel, Switzerland. This article is an open access article distributed under the terms and conditions of the Creative Commons Attribution (CC BY) license (https://creativecommons.org/licenses/by/4.0/).

1. Introduction

Fault systems are composed of combinations of faults with different properties that form within specific regional tectonic stress fields. They are among the most common structures in sedimentary basins and central to sedimentary basin analysis [1–3]. The spatial distribution, intersection, mechanical mechanisms, and displacement of faults are interrelated and reflect unified kinematic and dynamic conditions. Faults also record the structural evolution of fault-type oil and gas basins. Specifically, the temporal and spatial development of faults that control depressions greatly influence the structural evolution of basins and reservoir conditions [4–6].

The East China Sea Basin (ECSB) sits on the southeastern margin of the Eurasian Plate north of the South China Craton (Figure 1). It is bordered by the Zhejiang–Fujian uplift belt to the west and the Diaoyu Island fold belt to the east. The basin spans ~200–300 km in width from east to west, extends ~1500 km from north to south, and covers an area of 267,000 km^2 [7].

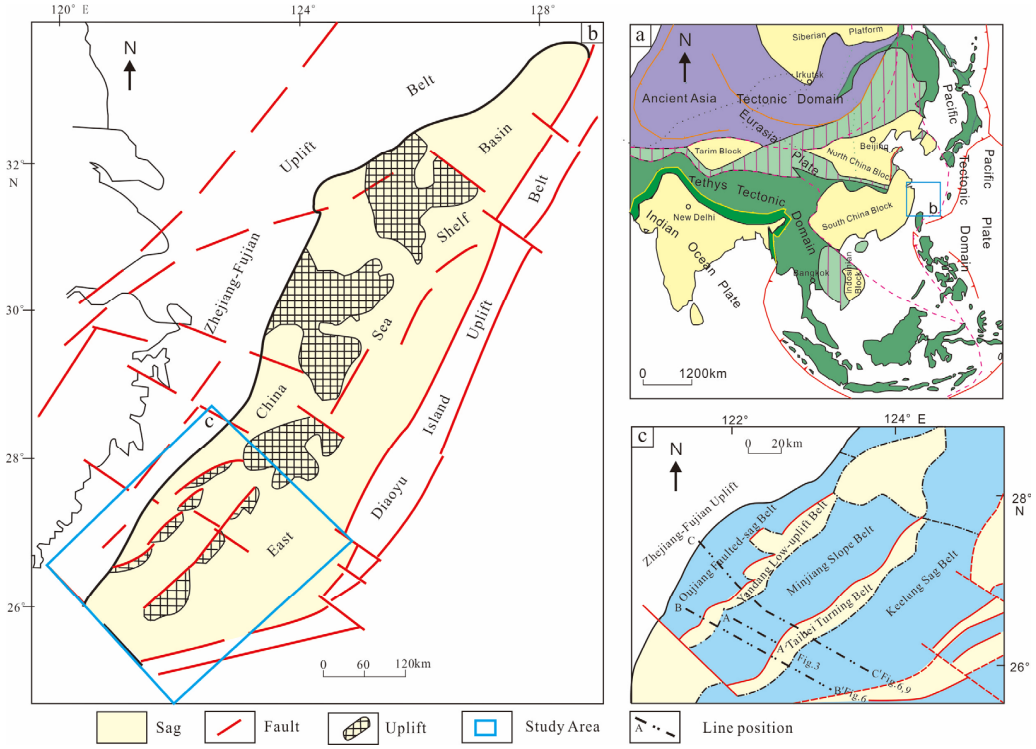


Figure 1. (**a**) Tectonic outline of Asia (after Refs. [8,9]), (**b**) regional tectonic map of the ECSB, and (**c**) Mesozoic structure of the SECSB.

The ECSB is one of the largest superimposed Mesozoic–Cenozoic oil basins in the East China Sea. With advances in exploration technology and theory, this Mesozoic basin has garnered recent attention, with much research on its stratigraphy [10–19], tectonic evolution [20–30], sedimentation [31–33], and hydrocarbon accumulation [34–39]. Studies have shown that the Mesozoic strata in the southern East China Sea Basin (SECSB) have potential for oil and gas exploration [40–43]. However, the structural characteristics and evolution of the Mesozoic faults in this basin, as well as their influence on hydrocarbon accumulation, remain poorly understood. Addressing these gaps is crucial for advancing oil and gas exploration in the ECSB.

In this study, recent oil and gas exploration results from the ECSB were employed for in-depth analyses of Mesozoic fault characteristics in the SECB. Based on structural interpretations, paleotectonic reconstructions, and comprehensive analyses of newly processed 2D seismic data, the results provide novel insights into the genesis and dynamic evolution of these faults. The influence of faults on hydrocarbon accumulation described here offers a foundation for oil- and gas-exploration decision-making in the region.

2. Geological Setting

The ECSB is bordered by the Pacific and Indian Plates [44]. This superimposed Mesozoic–Cenozoic basin developed atop an older craton, and its tectonic evolution is closely tied to the direction of movement of the Pacific Plate [45]. Consequently, the ECSB has undergone a complex tectonic evolution since the Mesozoic, with multiple stages of regional movement that have greatly impacted the development of its fault system.

According to the well data and land contrast analysis, the sedimentary basement of the ECSB consists of a biotite-rich dioritic gneiss from the Middle and Upper Proterozoic. This formation represents the metamorphic and crystalline basement of the Hercynian–Early Indo-Chinese period in South China. Wells LF1 and WZ6 in the Oujiang Fault zone revealed >300 m biotite–hornblende–plagioclase gneiss [7,29]. Drilling also revealed that the ECSB is composed of the Middle–Lower Jurassic Fuzhou, Upper Jurassic Xiamen, Lower Cretaceous Yushan, and Upper Cretaceous Minjiang and Shimentan

Formations [11–13] (Figure 2). The Fuzhou Formation includes dark-colored clastic rocks interbedded with thin layers of coal or carbonaceous mudstone. The Xiamen Formation consists of mixed-color clastic rocks. The Yushan Formation includes mixed-colored and reddish clastic rocks. The Minjiang Formation features brownish-gray, gray, light-gray, and tan mudstone interbedded with light-gray siltstone and sandstone and locally interbedded with grayish-black silty mudstone bands. The Shimentan Formation is characterized by brownish-red, brownish-purple, and dark brown mudstones interbedded with gray and grayish-white sandstone [11,13,19].

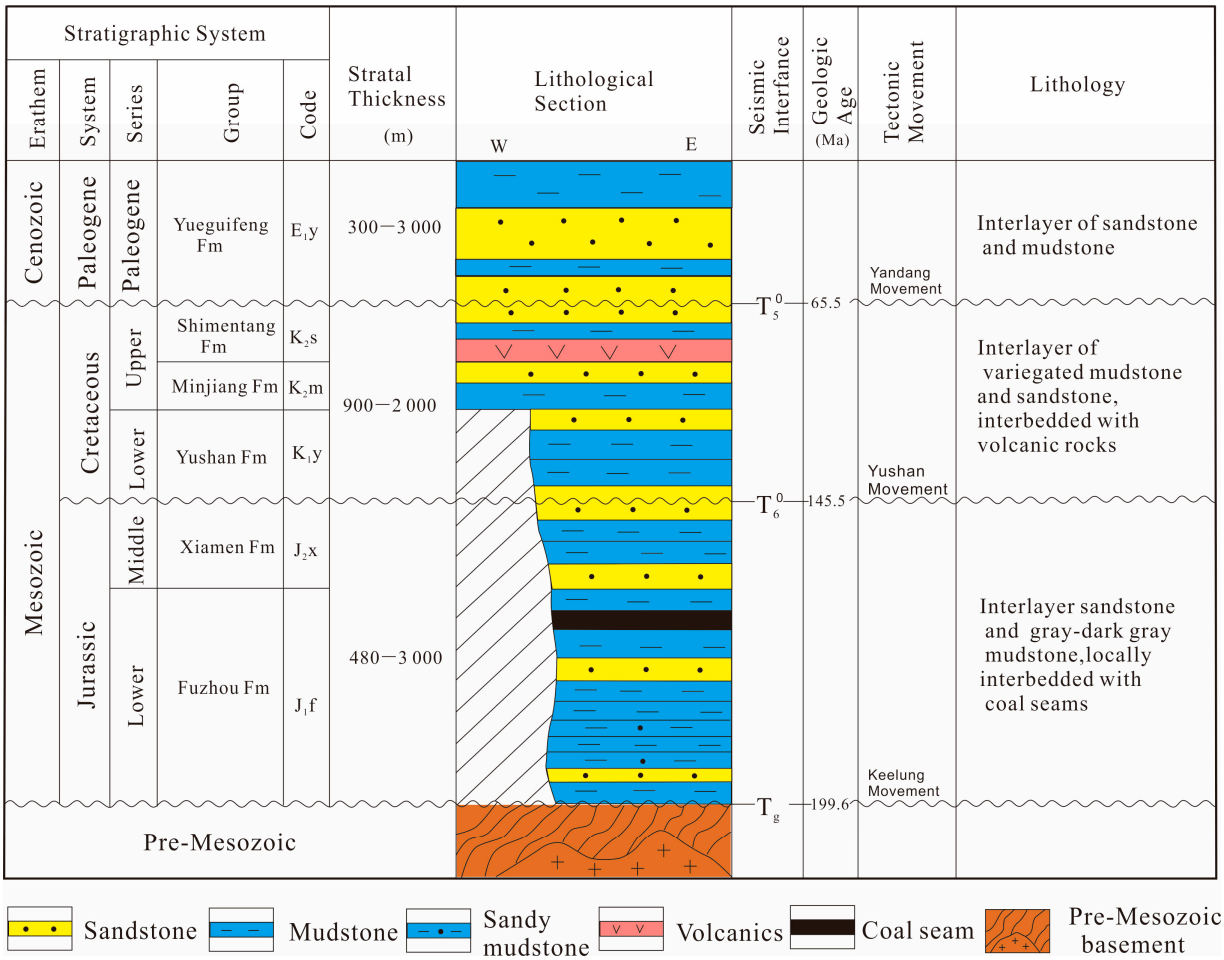


Figure 2. Mesozoic lithostratigraphy of the ECSB.

Based on seismic reflection characteristics, the Mesozoic can be divided into three seismic reflection interfaces (Tg, T_6^0, and T_5^0; Figure 2), which correspond to three unconformities. These unconformities are associated with regional tectonic movements (e.g., the Keelung, Yushan, and Yandang Movements) [16,17]. Through onshore–offshore correlations, it was determined that the main periods of tectonic movement were largely correlated. Specifically, the Keelung Movement is approximately equivalent to the Indosinian Movement, which coincides with the third episode of the Yanshan Movement, and the Yandang Movement aligns with the fifth episode of the Yanshan Movement [11].

Based on drill core and seismic profile data, Mesozoic strata are widely distributed across the study area, although their properties and thicknesses varied among tectonic units. Sedimentation is generally thicker in the east and thinner in the west, with the sedimentation center located in the east. In the western Oujiang sag belt, Cretaceous strata predominate, with thicknesses ranging from 500 to 1500 m, while Jurassic strata are largely absent [12,16,18]. The Yandang uplift belt contains both Cretaceous and Jurassic strata with

thicknesses ranging from 0 to 1000 m. In the central Minjiang slope and Taipei belt, the Jurassic and Cretaceous strata were ~2000–4000 m thick [12,16,18]. In the eastern Keelung sag belt, Jurassic and Cretaceous strata were ~4000–6000 m thick [10,12,16,18,19].

3. Materials and Methods

3.1. Data

The latest 2D seismic data from the study area were used. Owing to the complexity of the Mesozoic geological structure, fault development, and subsequent reformation, initial seismic data were of suboptimal quality, with weak seismic reflection energy, low frequency, and poor continuity. To address these issues, 2D seismic acquisition was performed using a long cable, strong source, high coverage, and deep amplification, along with a high-precision velocity modeling technique [46]. These methods greatly enhanced the reflection quality of the 2D seismic data in the East China Sea (Figure 3). The resultant dataset was of high quality and offered more detailed information for fault analysis.

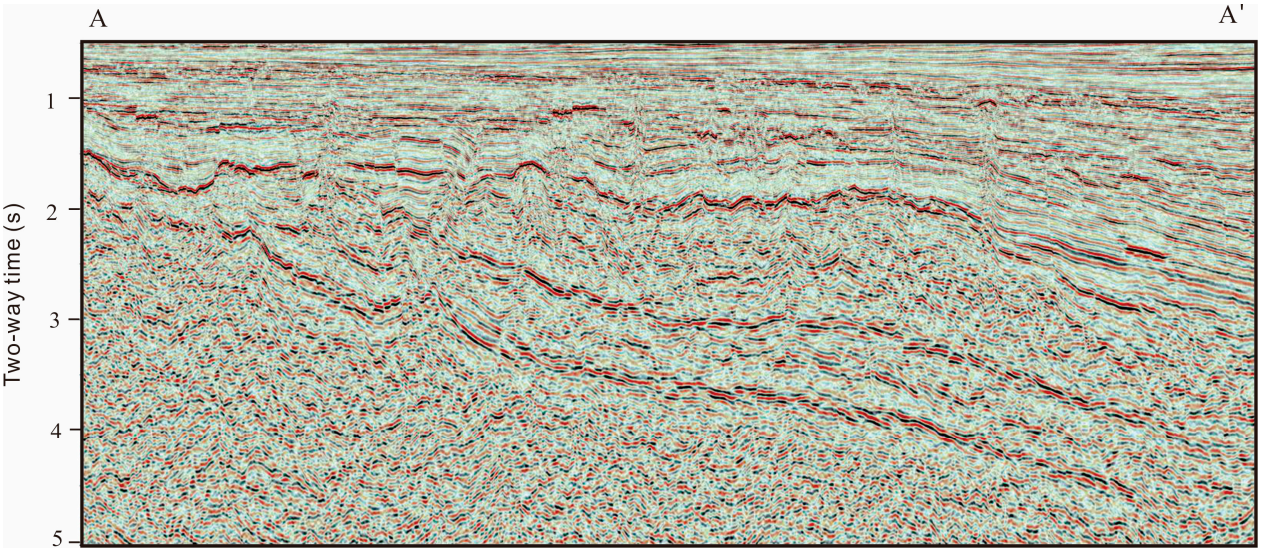


Figure 3. Seismic profile from newly acquired 2D data in the ECSB (A–A′ line location shown in Figure 1).

3.2. Methodology

3.2.1. Seismic Exploration

Seismic exploration technologies utilize seismic wave theory to record and analyze the responses of artificially generated seismic waves from subsurface media [47–49]. Seismic exploration is crucial for oil and gas exploration and development [50–52] and was used in this study to infer the spatial structure and rock properties of underground strata. Optimal acquisition parameters for Mesozoic strata in the ECSB were determined through simulations and 2D seismic acquisition tests. The parameters were as follows: a total source capacity of 95 120 cm^3, a cable length of 7500 m, a channel spacing of 12.5 m, a shot spacing of 37.5 m, a coverage parameter of 100-fold, a cable sinking depth of 8 m, and an air gun-sinking depth of 14 m [46]. Given the poor reflection quality and low signal-to-noise ratio of the original seismic data, noise suppression, ghost-reflection elimination, multiple attenuation, velocity analysis, and image-processing techniques were also employed [46,53–56]. These methods resulted in the generation of new and high-quality 2D seismic data.

3.2.2. Fault Growth Index

Since Thorsen [57] introduced the growth index (GI) in 1963, it has been widely used to study syntectonic faults within oil and gas basins. The key characteristic of syntectonic faults is the difference in thickness between downthrown and upthrown blocks. This

serves as the basis for the development of a fault growth index [57,58], which can reflect the relative velocity and age of two fault plates. Using the principles of sedimentary compensation, differences in strata of the same age between two fault plates can quantitatively reflect the occurrence and developmental processes of the fault [57–59]. The fault growth index is defined as the ratio of the thickness of the hanging wall (Hh) to that of the footwall (Hf) [57–64]:

$$GI = Hh/Hf \quad (1)$$

where GI = 1 indicates that the thicknesses of the two fault plates are equal and faulting stops. When GI > 1, the thickness of the hanging wall is greater than that of the footwall, reflecting synsedimentary normal faulting. When GI < 1, the thickness of the hanging wall is less than that of the footwall, reflecting the occurrence of reverse faulting.

3.2.3. Balanced-Profile Technology

A balanced cross-sectional technique was proposed in the 1950s [65] and 1960s [66]. This technique has subsequently found extensive applications in petroleum exploration and has undergone continuous refinement. Grounded in regional tectonic analysis, both geometric and kinematic principles are used to reconstruct structural deformations on geological cross-sections and their original states prior to deformation. This facilitates a better understanding of the evolutionary processes of geological structures [67–69].

Dhaslort [65,66] systematically discussed the balanced profile method, introducing two criteria for profile balance: layer length consistency and structural specificity. Elliott [67] subsequently proposed two test criteria: acceptability and rationality. A profile is considered balanced only if it satisfies all four of these conditions. Interpretation of a balanced profile also adheres to geometric rules, specifically the conservation of area and consistency in layer length, displacement, and fault-shortening [65–69].

Geological structures can often be reconstructed; however, the multisolution nature inherent to geological data leads to unique results. Consequently, balanced and restored sections cannot be directly equated. By utilizing extensive geophysical and geological data from the study area, an accurate geological profile interpretation can be achieved in this study. Subsequently, a balanced profile analysis was conducted to minimize the multiplicity of solutions [65–69].

4. Results

4.1. Fault Characteristics

4.1.1. Fault Plane Feature

The Mesozoic fault system in the SECSB predominantly trends NE–NNE, which aligns with the distribution of secondary tectonic units in the basin, while NW-trending faults are also present in some regions (Figure 4).

The extension lengths of these faults vary significantly, ranging from fault zones of up to 200 km to smaller faults spanning only several kilometers, and an average length of ~50 km. Faults are more developed in the western SECSB than in the eastern part. Table 1 presents the main fault elements.

Most Mesozoic faults in the SECSB are normal faults that were formed under tensile stress. Northeast–NNE-trending faults are the main structural controls in the basin and are characterized by their abundance, large scale, and wide distribution. The Mesozoic fault zone exhibits zonal characteristics oriented in an E–W direction. Western faults are well-developed, predominantly trending NE–NNE, while in the central area, faults are more developed and primarily trend NE, with additional NEE- and NW-oriented faults. In contrast, eastern faults are poorly developed. Common fault combinations include parallel, imbricated, and en echelon structures, with various morphological combinations (e.g., arborization).

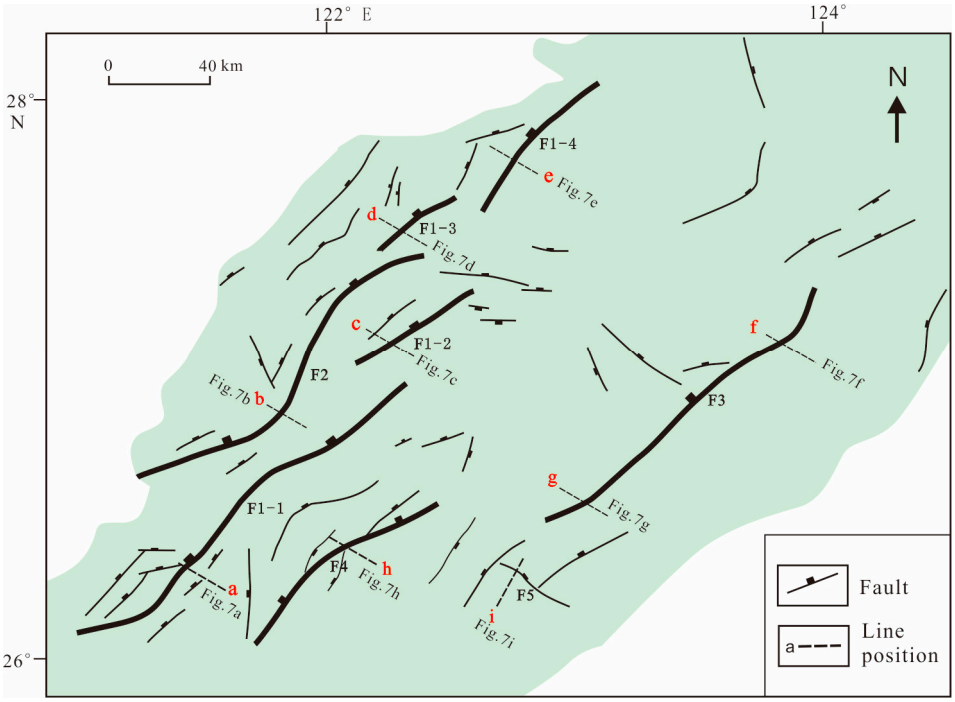


Figure 4. Distribution of Mesozoic faults in the SECSB.

Table 1. Main elements of Mesozoic faults in the SECSB.

Name	Properties	Vertical Distance (m)			Fault Occurrence		Length	Horizon
		T_5^0	T_6^0	T_g	Trend	Dip Tendency	Km	
F2	Normal Fault	1000–5000		300–6000	NE	NW	160	T_g T_5^0
F1-4	Normal Fault	1000–3000		1000–5000	NNE	NW	75	T_g T_5^0
F1-3	Normal Fault	1000–3000		1000–5000	NE	NW	38	T_g T_5^0
F1-2	Normal Fault	1000–3000		500–5000	NNE	NW	62	T_g T_5^0
F1-1	Normal Fault	500–2000		1000–3000	NNE	NW	150	T_g-T_5^0
F3	Normal Fault	500–1500	1000–2500	100–3000	NNE	NW	250	T_g-T_5^0

4.1.2. Fault Structure Styles and Vertical Characteristics

The Mesozoic of the SECSB was characterized by the superposition of multistage structural deformations, resulting in diverse fault structures. Fault structures can be classified into three primary types based on the influence of varying tectonic stress fields: extensional, compressional, and strike–slip, in addition to less common inversion faults. According to the classification of fault combinations, these structures can be subdivided into half-grabens, grabens, compressional anticlines, faulted anticlines, and flower structures (Figure 5).

Within different reflective layers of the same structural unit, the distribution of faults exhibited remarkable consistency and coordination, manifesting with similar strikes, directionalities, and geometric arrangements. Extensional faults were primarily developed within synrift basins, forming a series of half-grabens, grabens, and tilted blocks within sags induced by differential uplift and subsidence. Compressive faults formed primarily under compressive stress fields at the end of the Jurassic and were characterized by the development of compressive and fault anticlines within sags. In strike–slip faults, negative flower structures

predominantly developed on uplifts, whereas positive inversion structures formed within sags, largely under compressive stress fields at the end of the Jurassic.

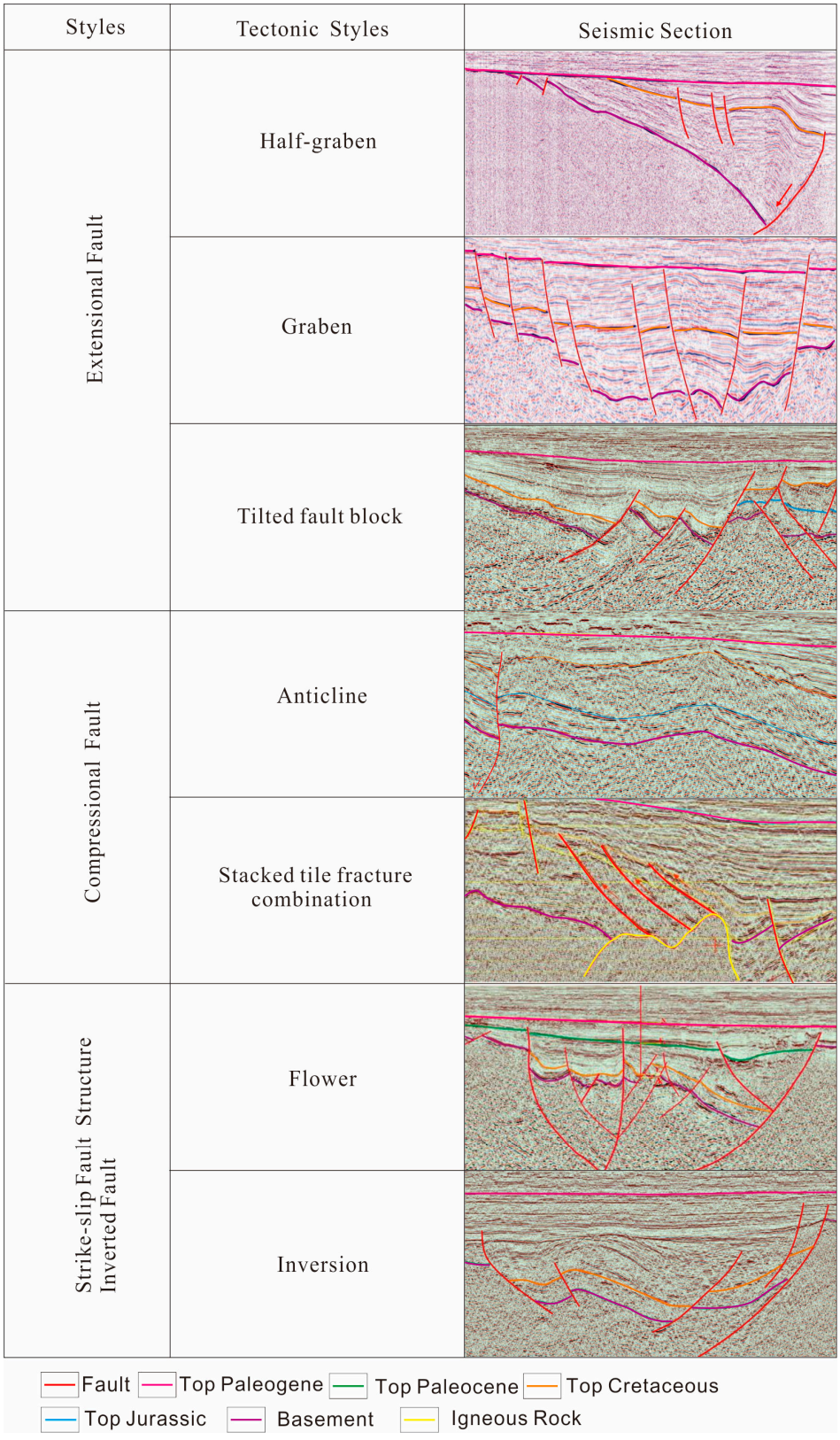


Figure 5. Tectonic structures of the Mesozoic SECSB.

4.2. Fault Divisions

Faults were categorized into two types, those controlling sag and uplifts and those controlling local structures, based on their distributions and scales.

4.2.1. Sag and Uplift-Controlling Faults

Faults controlling sags and uplifts exhibited NE–NNE strikes, wide distributions throughout the study area, and notable directionality (Figure 4). For example, fault F1 consisted of four segments, F1-1, F1-2, F1-3, and F1-4, which extended over >200 km, with vertical fault distances ranging from 1000 to 5000 m (Table 1). These faults play a critical role in controlling secondary structural units and are characterized by the symbiosis of fault and rift zones (Figure 6).

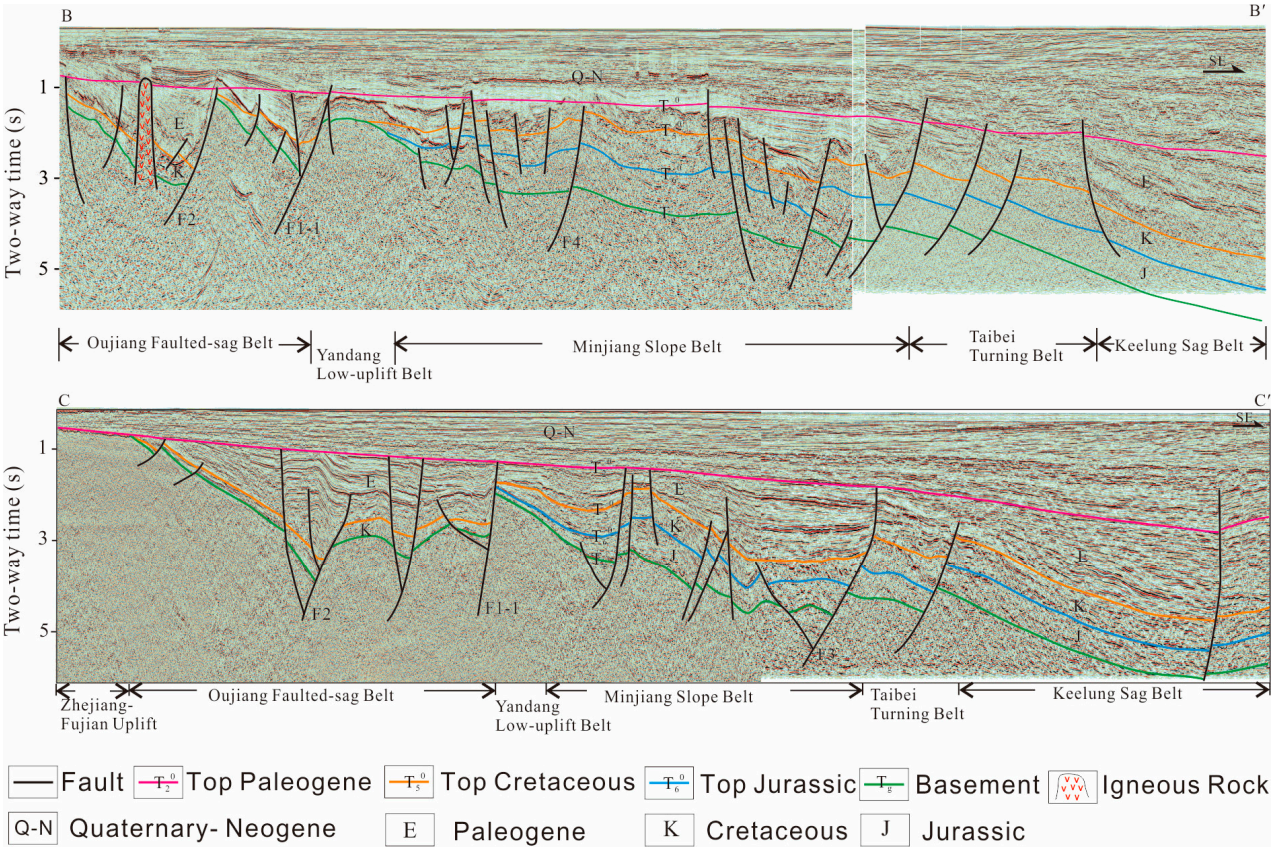


Figure 6. Mesozoic seismic transect across the SECSB (B–B′ line, C–C′ line location shown in Figure 1).

The Oujiang faulted-sag zone is governed by the west-dipping normal faults, F1-1, F1-2, F1-3, and F1-4, which are arranged in echelons. This configuration formed a dustpan-shaped depression with an eastern fault and western overlap (Figure 7a,c–e). Fault F2, which developed within the sag, further divided the area into two sub-sags in the east and west (Figure 7b). The Yandang low-uplift belt was situated on the upper side of the F1-1, F1-2, F1-3, and F1-4 faults. It comprised three ancient en echelon uplift zones and is distributed in an NE-trending, strip-like manner, with a W–E slope. The Taibei turning zone, located on the upper side of fault F3 (Figure 7f,g), extended NE and sloped from west to east.

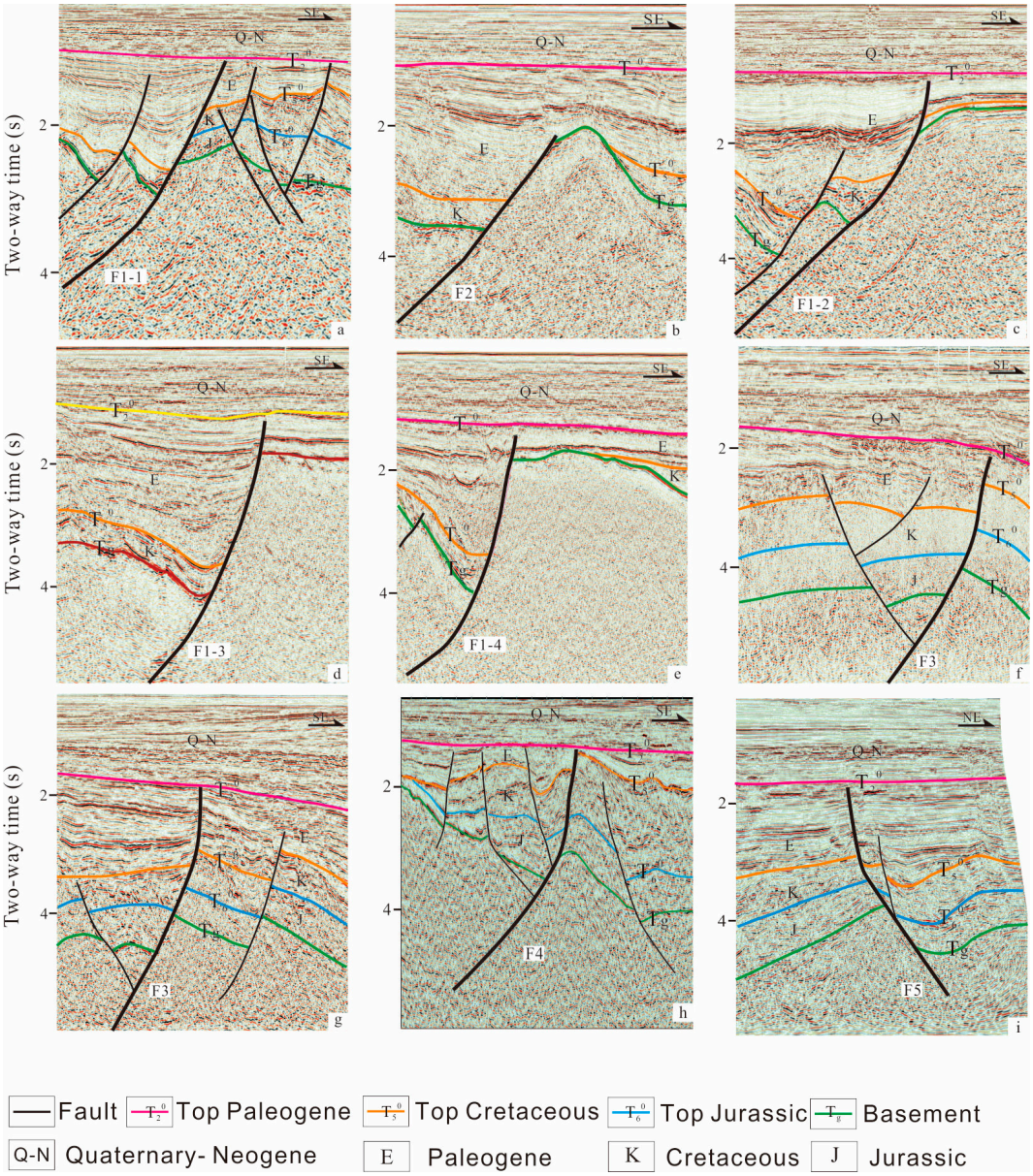


Figure 7. Characteristics of Mesozoic faults in the SECSB ((**a**–**i**) line location shown in Figure 4).

4.2.2. Local Structure-Controlling Faults

Faults that control local basinal structures primarily formed during the Yanshan–Himalayan epochs developed within the steep wing of the local structure and greatly influenced the occurrence and evolution of the local structures. The extension of the fault is directional and predominantly occurred within the sag. For instance, fault F4 had a typical strike of NE–NEE, with an extension length of 87 km, and was the principal fault controlling the local structures in the sag (Figure 7h). Conversely, fault F5, with a NW strike and an extension length of up to 33 km, governed local uplift structures (Figure 7i).

5. Discussion

5.1. Stages of Fault Activity and Evolutionary Characteristics

5.1.1. Period of Active Faulting

Variations in the GI and period of activity for faults F1, F2, and F3 were analyzed (Figure 8). For fault F1, GI > 1 during the Cretaceous, Paleocene, and Eocene–Oligocene sedimentary periods, remained consistently high in the Cretaceous and Paleocene, indi-

cating peak activity, with reduced activity in the Eocene–Oligocene. Fault F2 showed a maximum GI during the Cretaceous, signifying strong activity. Although it was still active during the Paleocene, its activity had diminished. By the Eocene–Oligocene, fault F2 had ceased to be active. Fault F3 had a GI > 1 throughout the Jurassic, Cretaceous, Paleocene, and Eocene–Oligocene periods, suggesting fault initiation in the Jurassic, peak activity in the Cretaceous, and reduced activity in the Paleocene and Eocene–Oligocene. Overall, most of the fault activity in this area occurred during the Cretaceous and Paleogene, with the Cretaceous period being the most active.

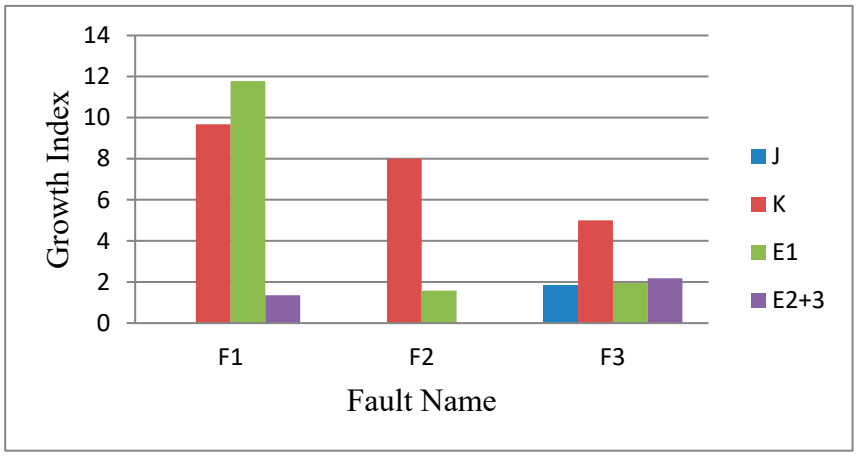


Figure 8. Growth indices of the three main Mesozoic faults (F1, F2, and F3) in the ECSB.

5.1.2. Tectonic Evolution

Owing to the largely rigid nature of the strata in the ECSB, a balanced section was constructed based on the principle of layer length conservation [55,56], which assumed that the true thickness was unchanged by deformation and that the lateral extent post-deformation was equivalent to that at the time of initial deposition. Applying this method, the seismic line C–C′, which traverses each sag in the study area, was selected to draw a balanced section.

During the Early–Middle Jurassic, the Izanagi Plate was subducted, compressed, and collided northwestward [70]. The basement strata on the eastern margin of the ECSB began to develop zones of shallow uplift under the compressional stress field, leading to the formation of depressions at the trailing edges of the uplift belts. These depressions evolved into subsidence zones that received Early–Middle Jurassic sediments [71]. At that time, no substantial faulting occurred in the basin (Figure 9). During the first episode of the Yanshan Movement at the end of the Middle Jurassic, the basin was widely uplifted, with a greater amplitude seen in the west than that in the east. This resulted in the extensive denudation of Early–Middle Jurassic sedimentary strata and the loss of Late Jurassic strata. The third episode of the Yanshan Movement, also known as the Yushan Movement, occurred at the end of the Late Jurassic. Due to the subduction of the Pacific Plate, the basement was uplifted, and thrusting occurred along the original collision zone. The thrust direction was NW–SW and formed an NE-trending reverse fault [72].

From the late Early Cretaceous to the Late Cretaceous, the retreat of the oceanic plate coupled with the northeastward subduction and collision of the Indian Plate [73] subjected the ECSB to tensile forces. This resulted in the formation of graben and half-graben structures, which greatly influenced sedimentation during this period. The depositional center was situated in the eastern part of the basin, specifically within the Keelung Depression, which the Minjiang slope overrode from E to W, resulting in the development of several secondary half-graben structures. During this period, the Oujiang fault depression also experienced deposition and was characterized by a half-graben structure controlled by three en echelon faults. The main boundary fault exhibited a steep upper section and gentle lower section, with eastward faults and a westward overlap. These faults likely extended

downward to the weak layer between the crust and mantle and exhibited tensional and torsion characteristics [71]. During the Jurassic, thrust faults that formed in compressional environments were predominantly reactivated as normal faults in subsequent stages. Consequently, imbricated thrust structures were only observed locally.

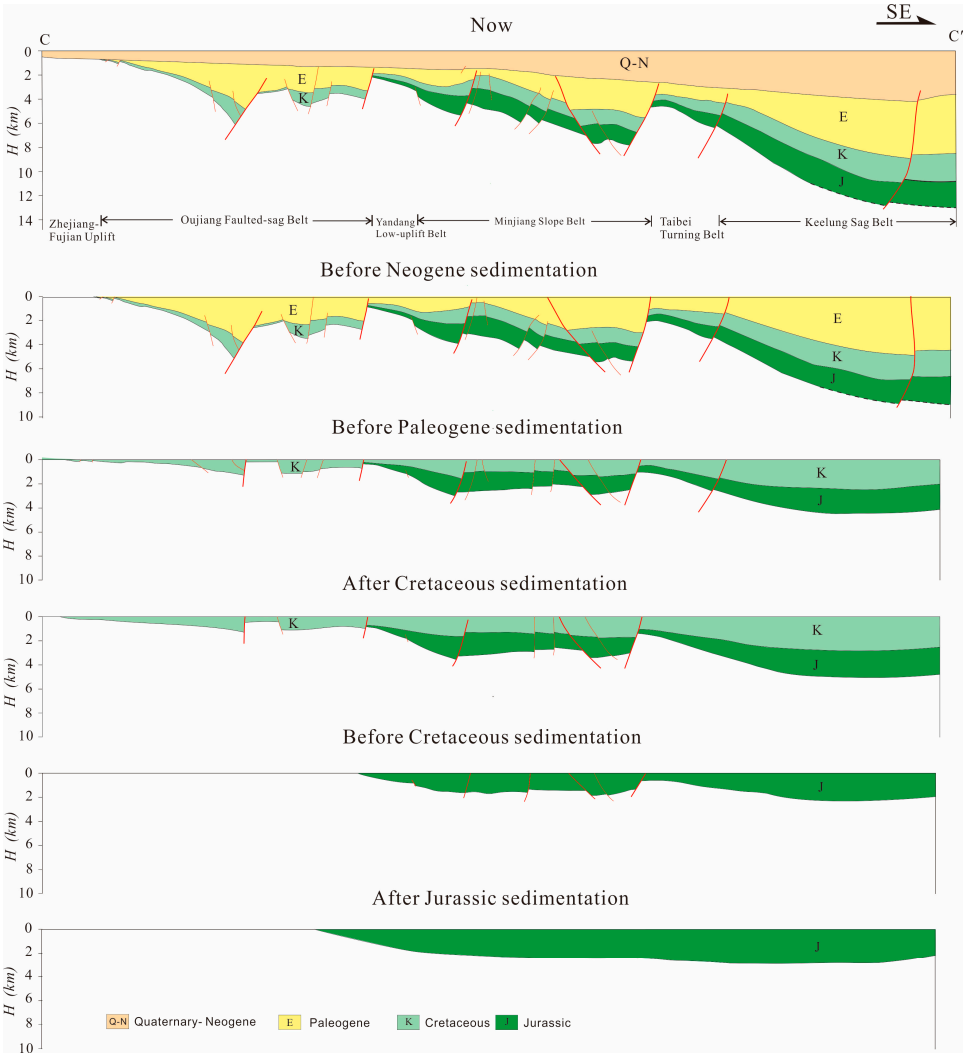


Figure 9. Evolution of the SECSB (C–C′ line location shown in Figure 1).

From the Late Cretaceous to the Eocene, the continental margin of East Asia underwent a complete transformation from an E–W to an NNE orientation. During this time, strike–slip pull-apart structures became more common, leading to the formation of a series of pull-apart basins [70]. Right-lateral en echelon faults and flower structures developed in the Oujiang fault depression and Yandang low uplift. Paleocene rifting initially formed in the western part of the basin as the angle of plate subduction steepened. Subsequently, an Eocene rift developed in the eastern part of the basin. During the Miocene, the entire ECSB subsided, transitioning from rift to regional depressional deposition [74].

5.2. Fault System and Hydrocarbon Accumulation

According to the reconstruction shown in Figure 9, the area of East China Sea hosted a typical rift basin during the Mesozoic era. Fault activity in the region was intimately linked to the generation, migration, and accumulation of oil and gas and played a key role in controlling these processes.

5.2.1. Controlling the Formation and Distribution of Hydrocarbon Source Rocks

Hydrocarbon source rocks in the ECSB predominantly formed during the Jurassic and Early Cretaceous. Fault activity, as the primary manifestation of tectonism, greatly influenced the formation and distribution of hydrocarbon source rocks. The Jurassic was characterized by depression-type deposits. Influenced by the first episode of the Yanshan Movement at the end of the Middle Jurassic, the strata experienced substantial denudation. The extent of denudation was greater in the west than it was in the east, with the maximum residual thickness observed in the Keelung sag belt [19]. During the Early Cretaceous, the Minjiang slope belt and Keelung sag belt extended eastward because of the subduction and retreat of the Izanagi Plate, resulting in the formation of graben and half-graben structures. The distribution of Jurassic source rocks was controlled by faults F3 and F4, which were formed via eastward extension. The thickness of dark mudstone ranged from 100 to 800 m [34] and was distributed northeastwardly (Figure 10).

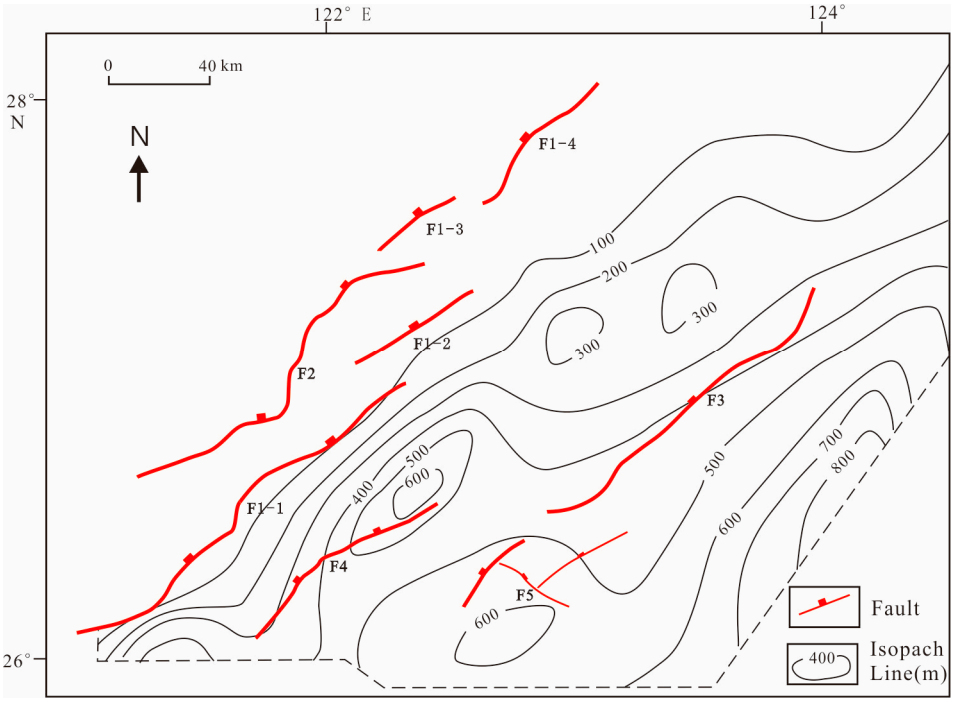


Figure 10. Thickness of Middle–Lower Jurassic dark mudstone in the SECSB (after Ref. [34]).

During the Cretaceous sedimentary period, the basin transitioned into a rifting stage because of the subduction of the Pacific Plate. Fault activity peaked during this time and remained high. Intense rifting facilitated the extensive development of hydrocarbon source rocks, with the thickness of dark mudstone ranging from 50 to 350 m [34]. The development and distribution of hydrocarbon source rocks were mainly influenced by faults F1 and F3, which extended along NE faults (Figure 11). The thickness of these source rocks gradually increased from the center of the central Minjiang slope belt toward the southeast of the study area, with a maximum thickness exceeding 350 m, centered in the Keelung sag belt. The predominant lithology is thick mudstone, representing bay and bathyal facies.

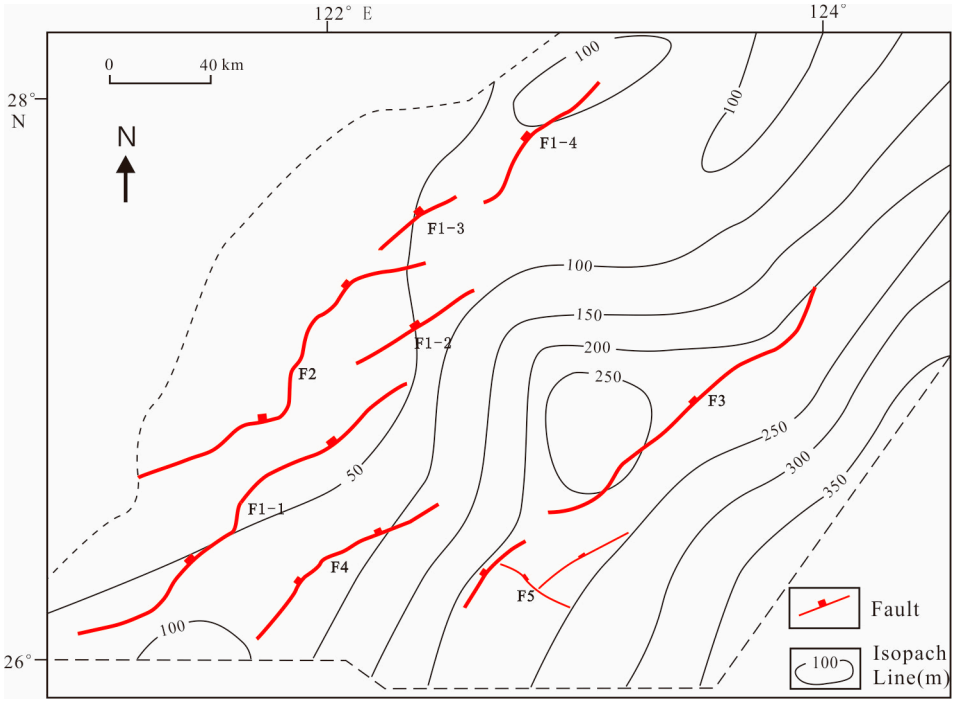


Figure 11. Thickness of Lower Cretaceous dark mudstone in the SECSB (after Ref. [34]).

5.2.2. Trap-Controlling Faults

Fault systems in the study area gave rise to various structures and associated traps, such as fault blocks, noses, and anticlines; buried hill drapes; and stratigraphic overlap traps. Their development and evolution primarily dictated the type, distribution, and timing of trap formation. Variations in fault configurations led to the development of different types of traps across the study area (Figure 12). Buried-hill drape traps mainly developed near the boundary faults of the control sag proximal to uplift. Stratigraphic overlap traps were primarily found on the slopes, whereas fault blocks and anticlines, as well as anticline traps, developed within the sags. Fault type also influenced the direction of traps, which generally aligned with the strike of the fault, exhibiting an NE or NNE strip-like pattern, regardless of whether the traps were located in an uplift, sag, or slope belt. Furthermore, compressional anticlines and faulted anticline traps formed during the compressional phases of the Late Jurassic and Late Cretaceous. During the pronounced extensional fault depression phase from the late Early Cretaceous to the Late Cretaceous, fault block and nose traps formed in depressions. Concurrently, buried-hill drape and stratigraphic overlap traps formed in the uplift and slope regions.

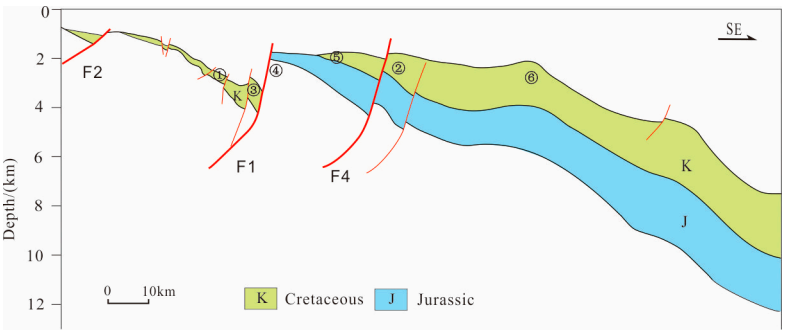


Figure 12. Schematic of trap types in the SECSB: 1 = fault block; 2 = fault nose; 3 = fault anticline; 4 = buried-hill drape; 5 = stratigraphic overlap; and 6 = anticline.

5.2.3. Influence on Hydrocarbon Migration and Accumulation

Since the Mesozoic, the ECSB has undergone four major fault movements—the Keelung, Yushan, Yandang, and Longjing. These movements influenced the evolution of the basin and the processes of oil and gas generation, migration, and accumulation. Mesozoic faults, sand bodies, and unconformities served as primary conduits for oil and gas migration. Their spatial distribution and relationships formed a conducting network for hydrocarbon systems. In particular, the spatial relationship among faults, reservoirs, and source rocks determined the characteristics of hydrocarbon accumulation.

Mesozoic faults F1, F2, F3, and F4 in the SECSB intersected Jurassic and Cretaceous strata and remained active from the Paleocene to the Oligocene. The Mesozoic was largely characterized by sandstone reservoirs formed on shallow sea shelves, in littoral shallow seas, and in deltaic channels. Their physical properties declined with increasing burial depth. At depths greater than 3100 m, these reservoirs are characterized by low porosity and permeability [75]. The Mesozoic hydrocarbon source rocks primarily belong to the Jurassic and Lower Cretaceous. These rocks exhibited secondary hydrocarbon generation characteristics, had a total hydrocarbon generation capacity of 1.2×10^{11} t, and were considered mature and effective hydrocarbon sources [36].

Hydrocarbon generation and expulsion from the Jurassic source rocks commenced in the Early Cretaceous and peaked during the Late Cretaceous. The Yandang Movement and the various traps formed prior to it were conducive to the accumulation and preservation of hydrocarbons. Faults and unconformities formed during the Yushan and Yandang Movements, which, respectively, occurred at the end of the Jurassic and Cretaceous, became the dominant channels for hydrocarbon migration. Jurassic deformation was weak, and reservoir connectivity was limited, which enabled the formation of self-sourced and self-contained oil and gas reservoirs.

Hydrocarbon generation and expulsion from the Lower Cretaceous source rocks commenced at the end of the Late Cretaceous and peaked at the end of the Paleocene. The Cretaceous sandstone reservoir exhibited excellent physical properties, with porosity ranging from 21.1% to 33% and a permeability of 787×10^{-3} μm^2 [76], indicating a high-porosity and high-permeability reservoir. Based on an analysis of fault activity, the Mesozoic era, particularly the Cretaceous, featured relatively intense faulting activity. The association between faults and sandstone facies facilitated hydrocarbon migration along the faults into sandstone reservoirs, resulting in self-generating and self-storing oil and gas reservoirs. Moreover, fractures and unconformities resulting from the Yandang Movement at the end of the Cretaceous and the Oujiang Movement at the end of the Paleocene facilitated the vertical migration of hydrocarbons, leading to the formation of lower-generation and upper-storage oil and gas reservoirs.

During the Late Eocene to Oligocene, substantial fault activity either generated numerous new tensional faults or reactivated preexisting tensional faults. This activity facilitated the remigration of the original oil and gas deposits beneath the regional caprock of the Mingyuefeng Formation [75] and led to the accumulation of hydrocarbons, as well as the formation of reservoirs. It also established a reservoir formation model characterized by Early Mesozoic formation reservoirs and late adjustment in the SECSB.

6. Conclusions

Based on analyses of the stages of active faulting and the relationships among faults and stratigraphic incised areas, it was concluded that the primary periods of activity were the Yanshan and Himalayan epochs. No prominent faulting occurred during the Jurassic. However, the development and sedimentary thickness of the Cretaceous were largely influenced by Yanshanian faults. The Yanshanian fault was primarily tensional and served as the principal fault responsible for local rifting and the formation of sags and uplift.

The primary hydrocarbon source rocks of the Mesozoic were from the Jurassic and Lower Cretaceous. Their distribution was predominantly influenced by tensile faults F1, F3, and F4. These rocks were located along the downthrown sides of faults and formed an

NE-trending source area. Fault systems developed during the Mesozoic, resulting in the formation of seven distinct structural styles and six types of traps. A series of structural belts, including the Oujiang fault depression, Yandang low-uplift, and Taibei turning belt, were distributed along the ascending wall of the hydrocarbon source area. These belts created favorable conditions for the migration and accumulation of hydrocarbons.

Since the Mesozoic, the ECSB has undergone four main tectonic movements—the Keelung, Yushan, Yandang, and Longjing—which played a key role in the evolution of the basin and greatly influenced the generation, migration, and accumulation of oil and gas. Mesozoic faults, sand bodies, and unconformities served as primary conduits for oil and gas migration during the Mesozoic. Based on an analysis of the spatial relationships among faults, reservoirs, and source rocks, self-generating and self-storing reservoirs were formed during the Mesozoic, along with rare lower-generating and upper-storing reservoirs. During the Late Eocene to Oligocene, intense fault activity either generated numerous new or reactivated existing tensional faults. This tectonic activity facilitated the remigration of the original oil and gas deposits, leading hydrocarbon accumulation and reservoir formation, supporting a model of reservoir formation characterized by Early Mesozoic reservoir formation and late adjustment in the SECSB.

Author Contributions: Conceptualization, Y.Y., J.W. and Q.Z.; methodology, J.S. and J.L.; writing—original draft, Y.Y., J.L. and C.Y.; writing—review and editing, Q.Z.; supervision, J.L. All authors have read and agreed to the published version of the manuscript.

Funding: This research was funded by the Laoshan Laboratory (grant nos. LSKJ202203401 and LSKJ202203404), the China Geological Survey (project nos. DD20221723, DD20230317, DD20230401, and DD20241723), the National Natural Science Foundation of China (grant nos. 41776075, 42076220, and 42206234), the Shandong Fund Project (grant nos. ZR2020QD038 and ZR2022MD054), and the Major Basic Research Projects of Shandong Province (grant no. ZR2021ZD09).

Institutional Review Board Statement: Not applicable.

Informed Consent Statement: Not applicable.

Data Availability Statement: All data and materials used in this study are available upon reasonable request made to the corresponding author.

Conflicts of Interest: The authors declare that there are no conflicts of interest.

References

1. Zhang, H.F.; Fang, C.L.; Gao, X.Z.; Zhang, Z.H.; Jiang, Y.L. *Petroleum Geology*; Petroleum Industry Press: Beijing, China, 1999.
2. Xu, L.L.; Fan, C.W.; Li, M.; Li, H.; Xu, B.; Cheng, Y.J.; Wu, Z.P. Characteristics and evolution process of Cenozoic fault system in the western area of Wenchang A sag, Pearl River Mouth basin. *China Offshore Oil Gas* **2024**, *36*, 37–48. [CrossRef]
3. Guo, Q.J.; Deng, M.Z.; Zhang, C.Y.; Shan, S.Q.; Ni, C.H.; Wang, B. Structural styles and their geological significance to petroliferous basins of China. *Oil Gas Geol.* **2024**, *45*, 609–621. [CrossRef]
4. Würtzen Camilla, L.; Alvar, B.; Miquel, P.M.; Mulrooney Mark, J.; Line lina, H.; Lvar, M. Impact of faulting in depocentres development, facies assemblages, drainage patterns, and provenance in continental half-graben basins: An example from the Fanja Basin of Oman. *Basin Res.* **2022**, *35*, 705–743. [CrossRef]
5. Park, J.; Lee, J.-H.; Hong, J. Tectono-sedimentary development of early synrift half-graben subbasins in the Miocene Pohang Basin, southeastern Korea. *Basin Res.* **2022**, *34*, 2135–2161. [CrossRef]
6. Fu, Q.M.; Liu, X.F.; Yao, J.L.; Wang, Y.B. Characteristics of Source Rocks and Formation of Reservoir Bitumen in Yinchuan Graben, Ordos Basin, China. *Energies* **2022**, *15*, 4809. [CrossRef]
7. Zhu, J.J.; Wang, Q.; Liang, J.S.; Wang, H.; Tian, B.; Hao, L.W. Cenozoic geological structure and tectonic evolution of southern East China Sea shelf basin. *Nat. Gas Geosci.* **2012**, *23*, 222–229. (In Chinese with English Abstract)
8. Ren, J.S.; Zhao, L.; Xu, Q.Q.; Zhu, J.B. Global tectonic position and geodynamic system of China. *Acta Geol. Sin.* **2016**, *90*, 2100–2109. (In Chinese with English Abstract)
9. Yang, C.Q.; Sun, J.; Yang, Y.Q.; Yang, C.S.; Wang, J.Q. Key factors controlling Mesozoic hydrocarbon accumulation in the Southern East China Sea Basin. *Mar. Pet. Geol.* **2020**, *118*, 104436. [CrossRef]
10. Wang, M.J.; Zhang, Y.; Pan, J.; Huang, L.; Chen, X.H.; Luo, D.; Hou, F.H.; Shang, L.N. Geological structure of the large section in eastern China's sea areas and its constraint on comprehensive stratigraphic division. *Geol. China* **2020**, *47*, 1474–1485. (In Chinese with English Abstract) [CrossRef]

11. Jiang, D.H.; Tang, J.; Wang, D.P.; Xu, L.M.; Li, G.; Yang, C.Q. Mesozoic stratigraphic framework of the southern East China Sea Shelf Ba sin and its correlation with adjacent areas. *Mar. Geol. Front.* **2017**, *33*, 16–21. (In Chinese with English Abstract) [CrossRef]
12. Cong, Y.; Liu, Z.; Lu, K.; Meng, X.J.; Zhang, X.F. Residual thickness of the Mesozoic in the Southern East China Sea Shelf Basin. *Mar. Geol. Front.* **2017**, *33*, 41–44. (In Chinese with English Abstract) [CrossRef]
13. Zhong, K.; Wang, X.F.; Zhang, T.; Zhang, M.Q.; Fu, X.W.; Guo, M. Distribution of residual Mesozoic basins and their exploration potential in the western depression zone of East China Sea Shelf Basin. *Mar. Geol. Quat. Geol.* **2019**, *39*, 41–51. (In Chinese with English Abstract) [CrossRef]
14. Wang, L.; Li, C.F.; Li, K.D.; Yao, Z.W.; Tao, T.S. Characteristics and tectonic implications of the Mesozoic residual strata in the East China Sea Shelf Basin. *J. Mar. Sci.* **2022**, *40*, 11–24. (In Chinese with English Abstract) [CrossRef]
15. Yang, C.S.; Yang, C.Q.; Yang, Y.Q.; Li, G.; Shang, L.N.; Han, B.F. Characteristics of Mesozoic strata in the East China Sea Shelf Basin and their geotectonic implications. *Period. Ocean Univ. China* **2017**, *47*, 86–95. (In Chinese with English Abstract) [CrossRef]
16. Yang, Y.Q.; Yang, C.S.; Li, G.; Yang, C.Q. Mesozoic recognition of East China Sea shelf basin and its distribution characteristics. *Pet. Geol. Eng.* **2016**, *30*, 5–13. (In Chinese with English Abstract)
17. Wang, W.J.; Li, G.; Yang, C.Q.; Yang, C.S. Charactristics of sesmic sequences in the East China Sea Shelf Basin and their geological attributes. *Mar. Geol. Quat. Geol.* **2013**, *33*, 117–122. (In Chinese with English Abstract) [CrossRef]
18. Li, G.; Gong, J.M.; Yang, C.Q.; Yang, C.S.; Wang, W.J.; Wang, H.R.; Li, S.Z. Stratigraphic features of the mesozoic "Great East China Sea": A new exploration field. *Mar. Geol. Quat. Geol.* **2012**, *32*, 98–104. (In Chinese with English Abstract) [CrossRef]
19. Jiang, Y.B.; Gong, J.M.; Cao, Z.M.; Li, G.; Yang, C.Q.; Yang, C.S. Correlation of the Mesozoic between Southern East China Sea shelf basin and its adjacent areas. *Mar. Geol. Front.* **2013**, *29*, 1–7. (In Chinese with English Abstract)
20. Hou, F.H.; Zhang, X.H.; Li, G.; Li, S.Z.; Wen, Z.H.; Li, R.H. From passive continental margin to active continental margin: Basin recordings of Mesozoic tectonic regime transition of the East China Sea Shelf Basin. *Oil Geophys. Prospect.* **2015**, *50*, 980–990. (In Chinese with English Abstract) [CrossRef]
21. Cui, X.; Wang, L.L.; Luo, H.M.; Huang, X.C.; Li, T.H.; Yang, C.S.; Dai, L.M.; Guo, L.L.; Ma, F.F.; Liu, Z. Sandbox modeling test for Mesozoic basins in Southern East China Sea Shelf Basin. *Mar. Geol. Quat. Geol.* **2017**, *37*, 181–192. (In Chinese with English Abstract) [CrossRef]
22. Liu, Z.; Dai, L.M.; Li, S.Z.; Guo, L.L. Mesozoic magmatic activity and tectonic evolution in the southern East China Sea Continental Shelf Basin: Thermo-mechanical modelling. *Geol. J.* **2018**, *53*, 240–251. [CrossRef]
23. Zhu, W.L.; Xu, X.H.; Wang, B.; Cao, Q.; Chen, C.F.; Gao, S.L.; Feng, K.l.; Fu, X.W. Mesozoic continental arc migration in southern China and its effects on the evolution of offshore forearc basins. *Earth Sci. Front.* **2022**, *29*, 277–290. (In Chinese with English Abstract) [CrossRef]
24. Wang, M.J.; Pan, J.; Gao, H.F.; Huang, L.; Li, X. Mesozoic basin evolution and hydrocarbon potential in the northern South China Sea and southern East China Sea. *Earth Sci. Front.* **2022**, *29*, 294–302. (In Chinese with English Abstract) [CrossRef]
25. Zhang, Y.; Yao, Y.J.; Li, X.J.; Shang, L.N.; Yang, C.P.; Wang, Z.B.; Wang, M.J.; Gao, H.F.; Peng, X.C.; Huang, L.; et al. Tectonic evolution and resource-environmental effect of China Seas and adjacent areas under the multisphere geodynamic system of the East Asia ocean-continent convergent belt since Mesozoic. *Geol. China* **2020**, *47*, 1271–1309. (In Chinese with English Abstract) [CrossRef]
26. Suo, Y.H.; Li, S.Z.; Zhao, S.J.; Somerville, I.D.; Yu, S.; Dai, L.M.; Xu, L.Q.; Cao, X.Z.; Wang, P.C. Continental margin basins in East Asia: Tectonic implications of the Meso-Cenozoic East China Sea pull-apart basins. *Geol. J.* **2013**, *50*, 139–156. [CrossRef]
27. Liang, X.X.; Chen, S.; Ma, B.S.; Liang, Y.Y.; Song, X.G.; Zhou, J.X.; Yu, Y.X.; Yu, L. Changes of tectonic regime of the East China Sea Shelf Basin since Mesozoic: Insights from the Tiantai slope belt, East China Sea. *J. Asian Earth Sci.* **2024**, *259*, 105900. [CrossRef]
28. Suo, Y.H.; Li, S.Z.; Cao, X.Z.; Wang, X.Y.; Somerville, L.; Wang, G.Z.; Wang, P.C.; Liu, B. Mesozoic-Cenozoic basin inversion and geodynamics in East China: A review. *Earth-Sci. Rev.* **2020**, *210*, 103357. [CrossRef]
29. Yang, C.Q.; Han, B.F.; Yang, C.S.; Yang, Y.Q.; Sun, J.; Yu, F.S. Mesozoic basin evolution of the East China Shelf and tectonic system transition in Southeast China. *Geol. J.* **2020**, *55*, 239–252. [CrossRef]
30. Yang, C.S.; Yang, C.Q.; Shang, L.N.; Yan, Z.H.; Yang, Y.Q. Discovery of Late Cretaceous-Paleocene faulted basins developed on the Yandang Low Uplift, East China Sea Shelf Basin. *China Geol.* **2019**, *2*, 243–244. [CrossRef]
31. Wang, J.; Li, Z.G.; Cai, L.X.; Gong, Q.Y. Sedimentary model of Mesozoic in the southern part of the East China Sea Shelf Basin. *J. Jilin Univ. (Earth Sci. Ed.)* **2019**, *49*, 131–138. (In Chinese with English Abstract) [CrossRef]
32. Hu, W.B. *The Mesozoic Sedimentary Systems in the Southern East China Sea Shelf Basin*; China University of Geosciences: Beijing, China, 2012; pp. 21–77. (In Chinese with English Abstract)
33. Li, Z.G.; Gong, J.M.; Cao, Y.C.; Wang, J.; Wang, W.C.; Li, G. Comparison of sedimentary characteristics of the Mesozoic in southern East China Sea and djacent uplifting areas. *Mar. Geol. Quat. Geol.* **2015**, *35*, 29–35. (In Chinese with English Abstract) [CrossRef]
34. Wang, M.J.; Xiao, G.L.; Yang, C.Q.; Yang, Y.Q.; Chen, X.; Huang, L. Characteristics and evaluation of Mesozoic source rocks in the southeastern East China Sea continental shelf. *China Geol.* **2019**, *2*, 133–141. [CrossRef]
35. Xiao, G.L.; Yang, C.Q.; Sun, J.; Yang, C.S.; Yang, Y.Q. Comparative study on geological conditions of Mesozoic oil and gas accumulation in Southern East China Sea Shelf Basin and central and southern Ordos. *Mar. Geol. Front.* **2021**, *37*, 77–80. (In Chinese with English Abstract) [CrossRef]

36. Xiao, G.L.; Wang, M.J.; Yang, C.Q.; Pang, Y.M. Numerical simulation of Mesozoic hydrocarbon generation, migration and accumulation in the southern East China Sea. *Mar. Geol. Quat. Geol.* **2019**, *39*, 138–149. (In Chinese with English Abstract) [CrossRef]
37. Wang, D.P.; Li, H.H.; Lu, Y. Geochemical characteristics and distribution of Mesozoic hydrocarbon source rocks in the southern part of East China Sea. *Offshore Oil* **2015**, *35*, 1–6. (In Chinese with English Abstract) [CrossRef]
38. Liu, J.; Xie, R.; Xu, M.; Lin, X.Y. Hydrocarbon accumulation model of the Mesozoic in Taibei Depression, East China Sea. *Mar. Geol. Quat. Geol.* **2019**, *39*, 150–158. (In Chinese with English Abstract) [CrossRef]
39. Yang, C.Q.; Li, G.; Gong, J.M.; Yang, C.S. Petroleum geological conditions and exploration prospect of the Mesozoic in southeast China Sea area. *J. Jilin Univ. (Earth Sci. Ed.)* **2015**, *45*, 1–12. (In Chinese with English Abstract) [CrossRef]
40. Liang, R.B. Analysis of hydrocarbon exploration potential in the Mesozoic of the southern East China Sea Shelf Basin. *Offshore Oil* **2017**, *37*, 16–22. (In Chinese with English Abstract) [CrossRef]
41. Jin, C.S.; Qiao, D.W.; Xu, X.H.; Li, G.; Liang, J.S.; Jiang, Z.X.; Xu, L.M. Oil and gas potential and target selection in southern East China Sea Shelf Basin. *Geol. China* **2015**, *42*, 1601–1609. (In Chinese with English Abstract)
42. Zhang, Y.G.; Chen, J.W.; Gong, J.M.; Liang, J.; Liao, J.; Wang, J.Q.; Yang, C.Q.; Zhao, Q.F.; Sun, J.; Yang, C.S.; et al. Progress in Marine Oil and Gas Survey in Qingdao Institute of Marine Geology over the past 45 years. *Mar. Geol. Quat. Geol.* **2024**, *44*, 2–23. [CrossRef]
43. Wang, M.J.; Chen, X.H.; Zhu, X.Q.; Huang, L.; Li, G.; Pan, J. Evolution and oil and gas resource potential of key sedimentary basins in the eastern China seas. *Mar. Geol. Front.* **2024**, *40*, 1–12. (In Chinese with English Abstract) [CrossRef]
44. Li, S.Z.; Zhao, G.C.; Dai, L.M.; Liu, X.; Zhou, L.H.; Santosh, M.; Suo, Y.H. Mesozoic basins eastern China and their bearings on the deconstruction of the North China Craton. *J. Asian Earth Sci.* **2012**, *47*, 64–79. [CrossRef]
45. Zang, S.X.; Ning, J.Y. Interaction between Philippine Sea Plate and Eurasia Plate and its influence on the movement eastern Asia. *Chin. J. Geophys.* **2002**, *45*, 188–197. (In Chinese with English Abstract)
46. Yang, C.Q.; Yang, C.S.; Yang, Y.Q.; Sun, J.; Yan, Z.H.; Yan, H.Y.; Zhang, S.Y.; Shi, J.; Yang, R. 2D seismic survey technology of Mesozoic "weak low frequency" reflection in the East China Sea shelf basin. *Mearine Geol. Front.* **2020**, *36*, 76–79. (In Chinese with English Abstract) [CrossRef]
47. Weatherby, B.B. The history and development of seismic prospecting. *Geophysics* **1940**, *5*, 215–230. [CrossRef]
48. Dobrin, M.B.; Dunlap, H.F. Geophysical research and progress in exploration. *Geophysics* **1957**, *22*, 412–433. [CrossRef]
49. Smith, N.J. Geophysical activity in 1963. *Geophysics* **1964**, *29*, 992–1014. [CrossRef]
50. Karcher, J.C. The reflection seismograph: Its invention and use in the discovery of oil and gas fields. *Lead. Edge* **1987**, *6*, 10–19. [CrossRef]
51. Levorsen, A.I.; Berry, F.A.F. *Geology of Petroleum*; WH Freeman: San Francisco, CA, USA, 1967.
52. Van Den Bark, E.; Thomas, O.D. Ekofisk: First of the giant oil fields in Western Europe. *AAPG Bull.* **1981**, *65*, 2341–2363.
53. Yan, Z.H.; Wang, X.J.; Liu, Y.Y.; Xu, H.N.; Yang, J.J.; Yang, C.Q.; Yang, C.S. Key techniques for multiple wave suppression in the East China Sea. *Mar. Geol. Front.* **2020**, *36*, 64–72. (In Chinese with English Abstract) [CrossRef]
54. Jiang, T.; Yan, Z.H.; Zhao, Q.; Fang, G. Discussion on deghost for multi-channel seismic survey in the East of China Sea. *Mar. Geol. Front.* **2017**, *33*, 58–63. (In Chinese with English Abstract) [CrossRef]
55. Yan, Z.H.; Wang, Y.; Li, P.F.; Qin, K. Research and application of multi-component seismic denoising based on Hilbert Huang transform. *Prog. Geophys.* **2015**, *30*, 2846–2854. (In Chinese with English Abstract) [CrossRef]
56. Wang, X.J.; Yan, Z.H.; Liu, J.J.; Yang, J.J. The application of formation Q value compensation method based on wavelet frequency division to the exploration of middle-deep hydrocarbon in the East China Sea. *Mar. Geol. Quat. Geol.* **2019**, *33*, 58–63. (In Chinese with English Abstract) [CrossRef]
57. Thorsen, C.E. Age of growth faulting in Southern Louisiana. *Trans. Gulf Coast Assoc. Geol. Soc.* **1963**, *13*, 103–110.
58. Lei, B. Review of methods with quantitative studies of activity intensiy of the growth fault. *Adv. Earth Sci.* **2012**, *27*, 947–956. (In Chinese with English Abstract)
59. Chen, G.; Dai, J.S.; Ye, X.S.; Rong, L.; Liang, Y. A comparison of the fault growth index with fault throw. *J. Southwest Pet. Univ.* **2007**, *29*, 20–23. (In Chinese with English Abstract)
60. Zhao, M.W. Discussion on the growth index of fault. *Exp. Pet. Geol.* **1989**, *11*, 250–254. (In Chinese with English Abstract)
61. Kang, H.Q.; Li, M.G.; Jia, H.C.; Yang, H.F.; Meng, J.L. Evaluation method of large boundary normal fault activity and its application. *Fault-Block Oil Gas Field* **2017**, *24*, 307–310. (In Chinese with English Abstract) [CrossRef]
62. Cao, G.S.; Li, R.; Bi, J.H.; Xu, G.M.; Xing, Z. Analysis on the growth index of fault in the southern Wulungu depression at early Mesozoic period. *J. Henan Polytech. Univ. (Nat. Sci.)* **2017**, *36*, 46–51. (In Chinese with English Abstract) [CrossRef]
63. Wang, H.Y.; Fu, X.F.; Wang, H.Z.; Chen, M.; Meng, L.D.; Ping, G.D. Research on the controlling effect of quantitative analysis and evaluation of fault activity on oil and gas accumulation in Qikou sag of Bohai Bay. *Acta Geol. Sin.* **2020**, *94*, 3062–3073. (In Chinese with English Abstract) [CrossRef]
64. Ran, W.M.; Luan, X.W.; Zhao, Z.F.; Liu, H.; Li, D.Y.; Zhao, Y.; Wang, H.D.; Yan, Z.H. Research on characteristics of growth faults in the southern East China Sea Shelf Basin. *Mar. Geol. Quat. Geol.* **2017**, *39*, 100–112. (In Chinese with English Abstract) [CrossRef]
65. Dahlstrom, C.D.A. Balanced cross sections. *Can. J. Earth Sci.* **1969**, *6*, 743–757. [CrossRef]
66. Dahlstrom, C.D.A. Structural geology in the eastern margin of the Canadian Rocky Mountains. *Bull. Can. Pet. Geol.* **1970**, *18*, 332–406.

67. Elliott, D. The construction of balanced cross-sections. *J. Struct. Geol.* **1983**, *15*, 101. [CrossRef]
68. Gibbs, A.D. Balanced cross-section construction from seismic sections in areas of extensional tectonics. *J. Struct. Geol.* **1983**, *5*, 153–160. [CrossRef]
69. Zhang, M.S.; Chen, F.J. Application condition of balanced-section technique and the case analysis. *Oil Geophys. Prospect.* **1983**, *33*, 532–540. (In Chinese with English Abstract) [CrossRef]
70. Yang, C.S.; Yang, C.Q.; Zhang, J.; Li, G.; Yang, Y.Q. Mesozoic tectonic styles and their dynamic mechanisms in the East China Sea Shelf Basin. *Mar. Sci. Bull.* **2017**, *36*, 431–439. (In Chinese with English Abstract) [CrossRef]
71. Yang, C.Q.; Yang, C.S.; Sun, J.; Yang, Y.Q. Mesozoic evolution and dynamics transition in southern shelf basin of the East China Sea. *J. Jilin Univ. (Earth Sci. Ed.)* **2019**, *49*, 139–153. (In Chinese with English Abstract) [CrossRef]
72. Zheng, Q.G.; Zhou, Z.Y.; Cai, L.G.; Lu, Y.D.; Cao, Q.G. Meso-Cenozoic tectonic setting and evolution of East China Sea shelf basin. *Oil Gas Geol.* **2005**, *26*, 197–201. (In Chinese with English Abstract)
73. Wan, T.F. *China Geotectonics*; Geology Pubishing House: Beijing, China, 2011; pp. 168–184. (In Chinese)
74. Feng, X.J.; Cai, D.S.; Wang, C.X.; Gao, L. The Meso-Cenozoic tectonic evolution in East China Sea Shelf Basin. *China Offshore Oil Gas (Geol.)* **2003**, *17*, 33–37. (In Chinese with English Abstract)
75. Yang, C.Q.; Sun, J.; Yang, C.S.; Yang, Y.Q.; Xiao, G.L. Hydrocarbon accumulation model of Mesozoic in Southern East China Sea Basin. *Mar. Geol. Front.* **2021**, *37*, 89–92. (In Chinese with English Abstract) [CrossRef]
76. Xu, X.H.; Chen, L.L.; Wang, Q.H. Analysis of Mesozoic geological characteristics and resource potential in the East China Sea Shelf Basin. *Offshore Oil* **2004**, *24*, 1–7. (In Chinese with English Abstract)

Disclaimer/Publisher's Note: The statements, opinions and data contained in all publications are solely those of the individual author(s) and contributor(s) and not of MDPI and/or the editor(s). MDPI and/or the editor(s) disclaim responsibility for any injury to people or property resulting from any ideas, methods, instructions or products referred to in the content.